Charge transfer dynamics of 3,4,9,10-perylene-tetracarboxylic-dianhydride molecules on Au(111) probed by resonant photoemission spectroscopy

Liang Cao,[1,2] Yu-Zhan Wang,[2] Tie-Xin Chen,[1] Wen-Hua Zhang,[1] Xiao-Jiang Yu,[3] Kurash Ibrahim,[4] Jia-Ou Wang,[4] Hai-Jie Qian,[4] Fa-Qiang Xu,[1,a)] Dong-Chen Qi,[2,3,b)] and Andrew T. S. Wee[2,c)]

[1]*National Synchrotron Radiation Laboratory, School of Nuclear Science and Technology, University of Science and Technology of China, Hefei, Anhui 230029, People's Republic of China*
[2]*Department of Physics, National University of Singapore, 2 Science Drive 3, Singapore 117542, Singapore*
[3]*Singapore Synchrotron Light Source, National University of Singapore, 5 Research Link, Singapore 117603, Singapore*
[4]*Beijing Synchrotron Radiation Laboratory, Institute of High Energy Physics, Chinese Academy of Sciences, Beijing 100039, People's Republic of China*

Charge transfer dynamics across the lying-down 3,4,9,10-perylene-tetracarboxylic-dianhydride (PTCDA) organic semiconductor molecules on Au(111) interface has been investigated using the core-hole clock implementation of resonant photoemission spectroscopy. It is found that the charge transfer time scale at the PTCDA/Au(111) interface is much larger than the C 1s core-hole lifetime of 6 fs, indicating weak electronic coupling between PTCDA and the gold substrate due to the absence of chemical reaction and/or bonding. © *2011 American Institute of Physics*. [doi:10.1063/1.3656834]

I. INTRODUCTION

In recent years, organic solar cells including organic photovoltaics and dye sensitized solar cells (DSSCs) have attracted considerable attention for applications in low-cost, large-scale, and flexible electronic devices.[1,2] In these devices, interfacial electron transfer dynamics is of critical importance for efficient solar energy conversion.[3] Ultrafast charge transfer at the organic/substrate interfaces, for example in systems consisting of nanostructured TiO$_2$ and organic dyes with strong electronic coupling,[4] is necessary to compete effectively against various loss processes, e.g., charge recombination at the interface, charge redistribution, and intramolecular thermalization of excited states.[5] Interfacial electron transfer largely depends on the electronic interactions or wavefunction overlapping between molecular states and the substrate conduction band. Molecular orientation and conformation at interfaces could also affect the electronic coupling between molecules and substrates.[6] For example, ultrafast interfacial electron transfer within several femtoseconds (fs) was observed for lying-down 4-fluorobenzenethiol monolayer on Au(111) as compared to the standing-up configuration of molecules with much slower charge transfer process, because the nearly parallel orientation of the molecular plane with respect to the Au(111) surface greatly enhances the electronic coupling between molecular π-electrons and metal *d*-bands.[7] Therefore, understanding molecular orientation and packing at interfaces and their influence on charge transfer dynamics is crucial for optimizing the device performance.

Among the most widely used organic semiconductor molecules, 3,4,9,10-perylene-tetracarboxylic-dianhydride (PTCDA), which consists of a perylene core and two anhydride functional groups, is a typical model planar molecule with excellent optoelectronic properties and chemical stability.[8,9] In particular, it forms highly ordered structures with lying-down geometry on various substrates, e.g., Au,[10,11] Ag,[12] HOPG,[13] NaCl,[14,15] and CuPc,[16] owing to the stabilizing effect of multiple intermolecular hydrogen bonding. The interfacial electronic structures and nature of interactions between PTCDA and the metal single crystal substrates such as Cu,[17] Ag,[17] Au,[18] and Ni,[17] have been systematically studied and compared.[9] It is found that PTCDA molecules are chemically bonded with Cu(100), Cu(110), and Cu(111) substrates. Moreover, molecular dissociation on Cu(100) has been reported.[19] For PTCDA on Ag(111), the perylene core extended π-electrons interact with the Ag(111) *d*-band electrons and its carboxylic oxygen atoms bond to the Ag atoms. The PTCDA/Au(111) interface, in contrast, is a weakly interacting interface dominated by van der Waals interactions. However, we cannot completely exclude the molecule-substrate chemical interaction, as a hybrid molecular gap state has been predicted by theoretical calculations.[20,21] Since the charge transfer dynamics at the organic/metal interface is closely related to the nature and strength of the interfacial interaction and electronic coupling, understanding the charge transfer dynamics at the PTCDA/Au(111) interface will help to clarify the nature of interactions at this interface.

Synchrotron-based resonant photoemission spectroscopy (RPES) has been successfully utilized to probe the ultrafast charge transfer dynamics at organic/inorganic interfaces using the core-hole lifetime as an internal reference clock.[4,22–33] This method allows the quantification of the delocalization of electrons from unoccupied molecular orbitals to a substrate with fs scale. Figure 1 depicts the working principle of RPES. In a typical x-ray absorption process [Fig. 1(a)] in molecules,
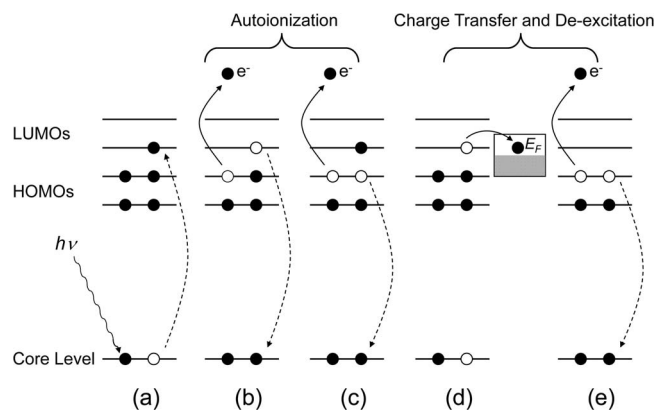
FIG. 1. Schematic overview of the working principle of RPES. Resonant excitation of a core level electron to the LUMOs (a) and the following competitive core-hole decay processes (b)–(e).

a core level electron (e.g., C 1*s*, N 1*s*) is excited to the lowest unoccupied molecular orbitals (LUMOs) and a core-hole is created. Two processes then compete within the specific core-hole lifetime, i.e., autoionization [Figs. 1(b) and 1(c)] and charge transfer [Fig. 1(d)]. The faster process will dominate. If the resonantly excited electrons are localized in the LUMOs and not transferred into the substrate conduction band within the core-hole lifetime, the core-hole will predominantly decay through the autoionization process. This is the typical scenario for organic multilayers since the molecules are usually isolated from the substrate surface. There are two autoionization channels, namely participator decay and spectator decay. In the participator decay [Fig. 1(b)], the resonantly excited electron fills the core-hole and a highest occupied molecular orbital (HOMO) electron is ejected by taking up the excess energy released by the decay process, leaving the system with a single HOMO hole. This final state is energetically equivalent to direct valence band (VB) photoemission by the incident photon, but the core-hole assisted resonant photoemission leads to larger cross section for the valence electrons, resulting in a resonant enhancement of the associated HOMO features in the photoemission spectrum. The resonant photoemission peak is constant in binding energy (BE) as the photon energy sweeps across the absorption edge. In the spectator decay channel [Fig. 1(c)], the excited electron remains in the LUMOs and does not take part in the de-excitation, and the decay proceeds via an Auger-like process with two HOMO electrons removed. Consequently, a new resonant Auger peak with constant kinetic energy (KE) will emerge at the lower BE side of the normal (non-resonant) one due to additional screening of the extra LUMO electron.

In contrast, if the molecular orbitals are strongly coupled to the substrate, the excited electrons can be transferred to the substrate conduction band through the interfacial charge transfer process [Fig. 1(d)] before the core-hole decay occurs, thereby leading to the normal Auger (non-resonant) process [Fig. 1(e)] without any enhanced resonant effects. Consequently, interfacial charge transfer competes with the decay processes of excited states via resonant photoemission or resonant Auger processes. In practice, the resonant photoemission experiment is carried out by acquiring a series of

photoemission spectra in the VB region by scanning the incoming x-ray photon energy across a specific absorption resonance feature. By comparing the RPES to near edge x-ray absorption fine structure (NEXAFS) spectroscopy intensity ratios at monolayer (coupled) and multilayer (isolated) thicknesses, the charge transfer time scale (τ_{CT}) from the LUMOs to substrate conduction band can be evaluated using Eq. (1).

$$\tau_{CT} = \tau_{CH} \frac{I_{RPES}^{mono}/I_{NEXAFS}^{mono}}{I_{RPES}^{multi}/I_{NEXAFS}^{multi} - I_{RPES}^{mono}/I_{NEXAFS}^{mono}}, \qquad (1)$$

where the intensities of LUMOs in the monolayer and multilayer PRES are denoted as I_{RPES}^{mono} and I_{RPES}^{multi}, respectively. I_{NEXAFS}^{mono} and I_{NEXAFS}^{multi} represent the intensities of LUMOs in NEXAFS, and τ_{CH} is the core-hole lifetime which has been measured as 6 fs for C 1*s*.[34] In particular, this technique is element and orbital specific, allowing selective studies of charge transfer dynamics for the elements and/or orbitals of interests. A thorough review on the principles and techniques of core-hole clock spectroscopy can be found in Ref. 35 by Brühwiler *et al*.

Here, we present a systematic study of the molecular orientation and charge transfer dynamics of PTCDA molecules on Au(111) using NEXAFS and RPES. Orientationally ordered PTCDA thin films with flat lying molecular geometry are observed at both the monolayer and multilayer regimes. Interfacial charge transfer time scale is found to be much longer than the core-hole lifetime of 6 fs, in accordance with the weak electronic coupling nature at the PTCDA/Au(111) interface.

II. EXPERIMENTAL DETAILS

A Au(111) single crystal was cleaned by repeated cycles of Ar$^+$ sputtering and annealing in ultrahigh vacuum (UHV). The cleanliness of the sample surface was checked by photoemission spectroscopy (PES). PTCDA molecules (Sigma-Aldrich) were thoroughly degassed for several hours before the sublimation using a standard Knudsen cell onto the Au(111) substrate at a deposition rate of 2 monolayer (ML)/min calibrated using a quartz crystal microbalance. The nominal deposition rate was also estimated using PES by the attenuation of the substrate Au 4*f* signal intensity.[36] The sample was kept at room temperature during and after PTCDA deposition.

Angular-dependent NEXAFS spectra were measured *in situ* at the 4B9B beamline of the Beijing Synchrotron Radiation Facility of High Energy Physics, Chinese Academy of Sciences. The C *K*-edge NEXAFS spectra were collected in total electron yield mode with a photon energy resolution of 200 meV. The linear polarization factor of the x-ray beam was measured to be better than 75%. The photon energy was calibrated using the characteristic intensity dip at 284.4 eV from the contamination carbon of the beamline optical components. To eliminate the fluctuations in the incident x-ray intensity and the extrinsic carbon absorption structures brought by the beamline optics, all NEXAFS spectra were first normalized to the incident photon intensity (I_0) monitored by the

refocusing mirror, and then they were divided by the clean Au(111) NEXAFS spectrum normalized to I_0.[37,38]

RPES and NEXAFS measurements were carried out *in situ* at the SINS beamline of Singapore Synchrotron Light Source equipped with a Scienta R4000 electron energy analyzer.[39] All measurements were performed at room temperature in a UHV chamber with a base pressure of 1×10^{-10} mbar. The photon energy was calibrated using the Au $4f_{7/2}$ core level peak at 84.0 eV of a sputter-cleaned gold foil in electrical contact with the sample. RPES spectra were measured at the VB region with photon energy swept across the C $1s \rightarrow \pi^*$ resonances, and plotted on a BE scale with respect to the substrate Fermi level (E_F). The intensities of the spectra were normalized using the incident photon intensity.

III. RESULTS AND DISCUSSION

A. Molecular orientation and ordering

Angular-dependent NEXAFS, which is an ideal tool to determine the adsorption geometry of planar aromatic molecules,[38] was performed at the C K-edge to study the molecular orientation of PTCDA molecules on Au(111). Figures 2(a) and 2(b) show the angular-dependent C K-edge NEXAFS spectra for monolayer and multilayer (10 ML) PTCDA molecules adsorbed on the Au(111), respectively, in which the x-ray incident angle θ is defined with respect to the substrate surface plane. Several distinct absorption resonances of PTCDA molecules can be clearly identified, which are in good agreement with previously reported NEXAFS spectra for PTCDA on other substrates.[40–42] The sharp resonances (peak $1 \sim 4$) below 290 eV are attributed to C $1s \rightarrow \pi^*$ transitions, whereas the broad absorption features at higher photon energy are assigned to C $1s \rightarrow \sigma^*$ transitions. Both the π^* resonances and σ^* resonances display significant change in the intensities with incident angle θ. For monolayer PTCDA, the π^* resonances are strongest at grazing incidence ($\theta = 20°$), whereas the σ^* resonances are strongest at normal incidence ($\theta = 90°$). Multilayer PTCDA spectra

show similar angular dependence. For planar π-conjugated organic molecules such as PTCDA, the π^* orbitals are essentially out of the molecular plane, and therefore the observed angular dependence indicates a nearly lying-down configuration of PTCDA molecular planes for both monolayer and multilayer coverages with high degree of orientational order, which is consistent with reported STM results for PTCDA on Au(111).[43–45]

To quantitatively evaluate the molecular orientation, the intensity of π^* resonances (I_{π^*}) at various incident angles (θ) can be related to the molecular tilt angle (α) by the following equation:[38,46]

$$I_{\pi*} = C P (\sin^2 \alpha \sin^2 \theta + 2 \cos^2 \alpha \cos^2 \theta)$$
$$+ C(1 - P)\sin^2 \alpha, \qquad (2)$$

where C is a normalization constant, P is the linear polarization factor of x rays (~ 0.75), and α is the average tilt angle of molecular plane with respect to the substrate surface plane. (see Fig. 2 inset)

Figure 3 plots intensities of the most intense π^* resonance (peak 2) for monolayer (open circle) and multilayer (cross) PTCDA as a function of θ together with the theoretical curves for different molecular tilt angles (solid line) generated using Eq. (2). The vertical error bars, which correspond to uncertainties introduced by the normalization and integration, are estimated to be within 10% of the intensities.[27] The average tilt angle α of PTCDA molecules on Au(111) was determined to be $21 \pm 10°$ for both monolayer and multilayer. The overall uncertainty in the estimated tilt angle takes into account the fitting errors, the degree of polarization of the x-ray beam and the angular misalignment due to sample mounting.[47] However, it should be noted that the
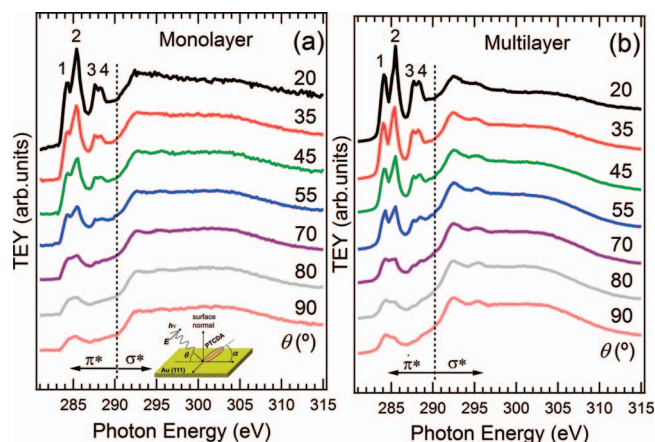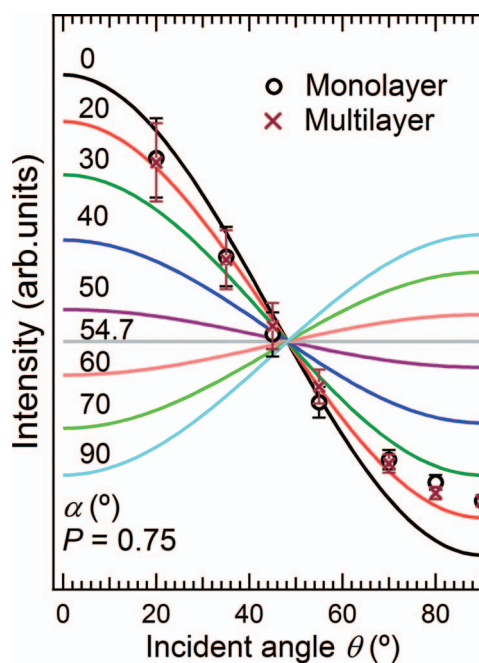

FIG. 2. Angular-dependent C K-edge NEXAFS spectra for monolayer (a) and multilayer (b) PTCDA molecules on the Au(111). The inset shows the measurement geometry.

FIG. 3. The intensities of the most intense π^* resonance (peak 2) against θ for monolayer (open circle) and multilayer (cross) PTCDA films on Au(111). The solid lines represent the theoretical angular dependence of π^* resonances for various molecular tilt angles.

tilt angle estimated from NEXAFS analysis is significantly overestimated, as STM studies point to a completely flat-lying adsorption geometry for PTCDA on Au(111).[43–45] Several factors, including tilted molecular species adsorbed at surface steps or defect sites,[40,48] thermal vibrations and/or distortion of molecular plane,[40,48,49] and the presence of non-$\pi*$ orbitals in the $\pi*$ excitation energy range,[48,50] may contribute to residue $\pi*$ intensities for the normal incident angle of x rays. In particular, the inclusion of non-π symmetry states in the LUMO (peak 1) energy region may account for the enhanced LUMO intensity for the multilayer PTCDA at normal incidence of x rays [Fig. 2(b)].[13,16]

B. Charge transfer dynamics

The relative alignment between the LUMOs of PTCDA molecules in their excited states and the E_F of the metal substrate is one of the most important factors that influence the charge transfer dynamics. Figure 4 shows the VB (occupied states) and NEXAFS spectra (unoccupied states) for monolayer and multilayer PTCDA on Au(111), along with the VB spectrum for the pristine gold substrate. The BE of 284.7 eV for perylene C $1s$ core level was adopted to place the NEXAFS spectra on a common BE scale along with the VB spectra,[51] where the dashed line marks the position of E_F.

At high molecular coverage, various molecular frontier orbitals including the highest occupied molecular orbital (HOMO), HOMO-1, HOMO-2, and HOMO-3 peaks derived from PTCDA molecules are clearly visible,[52,53] whereas the monolayer spectrum contains significant contributions from
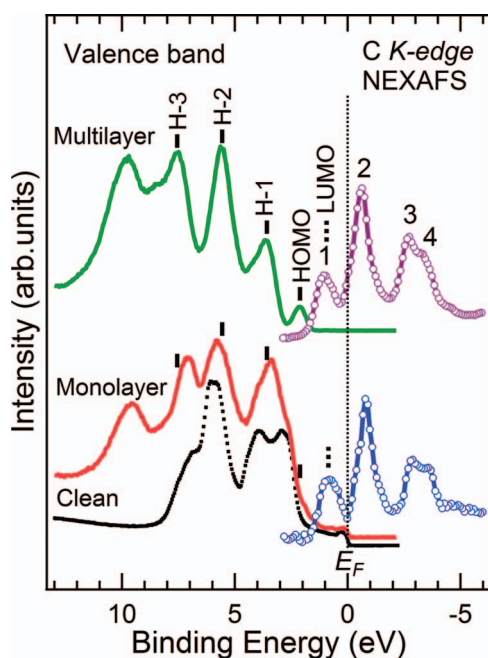

FIG. 4. VB and C *K*-edge NEXAFS spectra for monolayer and multilayer PTCDA on Au(111). The bottom spectrum (black dots) represents the VB spectrum for pristine Au(111) substrate. The relative BE scale of NEXAFS spectra was referenced to the C $1s$ (perylene core) core level BE of PTCDA molecules.

the gold substrate VB features. On the NEXAFS side, the lowest resonance (peak 1) is attributed to transitions from the perylene core carbon atoms to the LUMO, whereas the strong resonance (peak 2) corresponds to transitions from the perylene core to the next three higher orbitals (LUMO+1 $\sim$ LUMO+3). The resonances 3 and 4 originate from the anhydride C-atoms to LUMO and LUMO+1 $\sim$ LUMO+3 transitions, respectively.[40] For NEXAFS measurements, due to the Coulomb interaction between the core-hole and the photo-excited electron (i.e., excitonic effect), the measured NEXAFS resonances usually shift towards E_F or even below E_F.[54] As observed in the current PTCDA/Au(111) system, the LUMO lies below E_F of the Au(111) as shown in Fig. 4 for both monolayer and multilayer films. Consequently, electron transfer from the excited LUMO state of the molecules to the substrate conduction band is energetically unfavorable.[55] Therefore, only higher lying empty molecular orbitals (MOs) (e.g., LUMO+1 $\sim$ LUMO+3) can participate in the interfacial charge transfer.

RPES spectra for monolayer and multilayer PTCDA on Au(111) from 282 eV to 290 eV across the C $1s \rightarrow \pi*$ absorption threshold are shown in Fig. 5. The C $1s$ core level component excited by the second-order harmonic x-rays ($2h\nu$) was removed. In general, the resonant photoemission spectra for monolayer and multilayer PTCDA exhibit similar features: several resonant enhancements of photoemission features are clearly visible across the C *K*-edge absorption edge. Resonant features with lower BE (<8 eV) are mainly associated with the resonant enhancement of individual molecular frontier orbitals (HOMO $\sim$ HOMO-3) and they are relatively discrete in energy. On the other hand, broad resonant structures at higher BE (above 8 eV) are mostly contributed by the resonant Auger and normal Auger process.

It can be seen from Fig. 5 that the resonance photon energies correspond well with the four absorption features (peak 1 $\sim$ 4) in the NEXAFS spectra. For example, the HOMO and HOMO-1 derived features resonate at photon energies ranging from 283.4 eV to 286.6 eV associated with the $C_{perylene}$ $1s$ $\rightarrow$ LUMOs transitions, whereas they nearly vanish at higher photon energies corresponding to $C_{anhydride}$ $1s$ $\rightarrow$ LUMOs transitions. In particular, the HOMO-1 is most significantly enhanced at photon energies around 285–286.6 eV, corresponding to $C_{perylene}$ $1s$ $\rightarrow$ LUMO+1 $\sim$ LUMO+3 transitions. In addition, the HOMO-2 related resonance can be observed at all four $\pi*$ absorption peaks in the C *K*-edge NEXAFS, whereas the HOMO-3 derived resonance is much weaker in intensity at the $C_{anhydride}$ $1s$ $\rightarrow$ LUMOs transition region and can be barely observed at the other transition regions due to the large background signal contributed by the Auger structures on the higher BE side (also see Fig. S1 in supplemental material[56]). The observed dissimilar photon energy dependence for these resonant MO-derived VB features could be related to the wavefunction character and symmetry of the frontier MOs (HOMO $\sim$ HOMO-3): resonant photoemission arises only for specific photon energies that can excite core electron to LUMOs whose wavefunctions are spatially overlapping with that of the resonantly enhanced HOMOs.[57,58] In addition to these resonant photoemission features that are constant in BE, a resonantly enhanced Auger
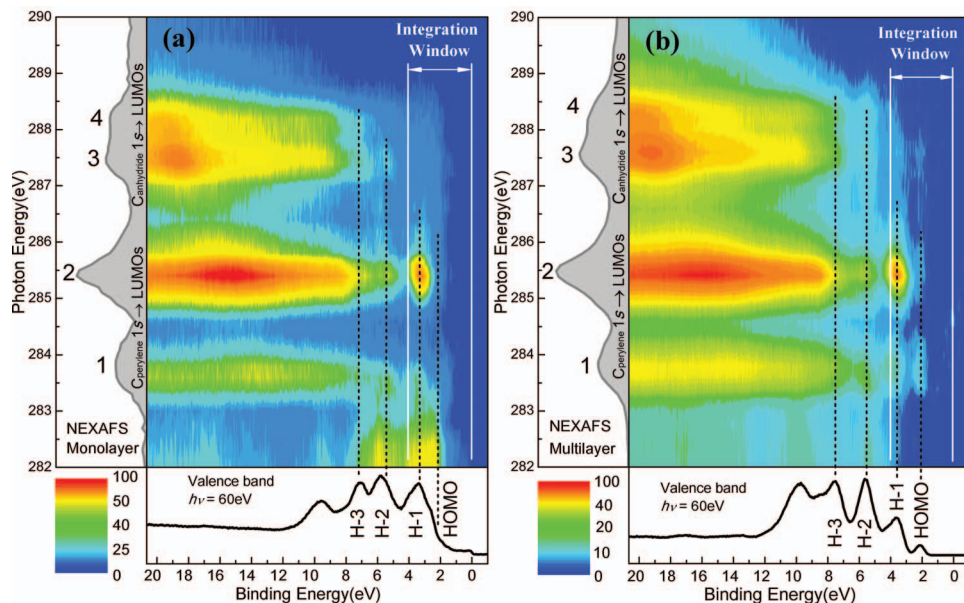
FIG. 5. RPES spectra for monolayer (a) and multilayer (b) PTCDA on Au(111). The bottom spectra are corresponding VB spectra measured with photon energy of 60 eV and the spectra on the left side is their respective NEXAFS spectrum.

peak due to the opening of spectator decay channel, which shows roughly linear dispersion in BE against the incident photon energy (i.e., constant KE), can also be observed in both monolayer and multilayer spectra (see Figs. S2 and S3 in supplemental material[56]).

The fact that significant resonant features resulting from the participator decay and spectator decay channels can be clearly resolved in both monolayer and multilayer PTCDA on Au(111) suggests that the photo-excited electrons are considerably localized in the molecules without obvious charge transfer to the substrate within the core-hole lifetime. This is in clear contrast to the thickness-dependent resonant photoemission profile observed in certain organic-metal systems with strong electronic coupling at the interface,[28] where the resonant photoemission features are greatly suppressed at monolayer coverage of organic molecules. Moreover, the similar resonant features, in particular the Auger-like autoionization signals, in monolayer and multilayer RPES spectra also indicate that no back-donation of electrons from substrate into the molecular LUMO states occurs either in the core-excited state or in the ground state. Otherwise a new superspectator decay channel will be opened up and additional spectator features with higher kinetic energy in RPES for monolayer film can be detected.[23,59] To determine the charge transfer time scale, the participator signal between 0 eV and 4 eV in BE including no Auger-type signal, e.g., spectator decay and normal Auger decay, are integrated as RPES spectra, which are plotted as a function of photon energy in Fig. 6, together with the corresponding NEXAFS spectra for monolayer and multilayer PTCDA, respectively. The background of monolayer integrated RPES spectrum contributed by the VB features of Au(111) substrate was subtracted using the clean Au(111) as a reference. The resonance profiles are both normalized with respect to the peak 1 height in NEXAFS. As can be seen in Fig. 6, the RPES/NEXAFS ratios (R) determined for

other LUMO peaks are $R_2^{\mathrm{multi}} = 1.36 \pm 0.01$, $R_2^{\mathrm{mono}} = 1.37 \pm 0.02$; $R_3^{\mathrm{multi}} = 0.28 \pm 0.02$, $R_3^{\mathrm{mono}} = 0.29 \pm 0.04$; and $R_4^{\mathrm{multi}} = 0.31 \pm 0.02$, $R_4^{\mathrm{mono}} = 0.31 \pm 0.04$. Within the error, the intensity ratio for each LUMO peak is hardly changed from monolayer to multilayer regime, and Eq. (1) is no longer valid for an estimation of the charge transfer time scale τ_{CT}.
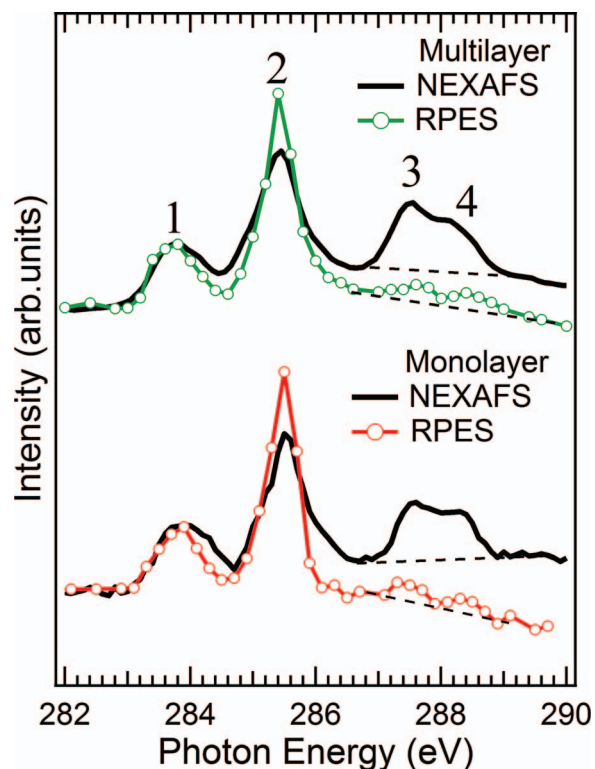

FIG. 6. Integrated RPES and the corresponding C K-edge NEXAFS spectra for monolayer and multilayer PTCDA molecules on Au(111). The dashed lines mark the background.

Considering Eq. (1) is largely valid for charge transfer time scale within one order of magnitude higher or lower than the respective core-hole lifetime (0.6 fs $< \tau_{CT} <$ 60 fs),[4,35] we can estimate 60 fs being the lower limit of the charge transfer time scale for PTCDA/Au(111) interface ($\tau_{CT} \gg$ 60 fs). This essentially indicates that the excited electrons remain localized in molecules, despite the fact that the lying-down geometry of molecules should facilitate interfacial charge transfer. The slow charge transfer dynamics for monolayer PTCDA on gold suggests weak electronic coupling and predominant van der Waals type interactions at the PTCDA/Au(111) interface, consistent with previous experimental findings. Consequently, although the weakly interacting gold substrate could potentially benefit the formation of highly ordered PTCDA overlayers, it may not be an ideal electrode for organic device applications owing to the slow charge transfer dynamics at this particular interface.

IV. CONCLUSIONS

We have systematically studied the molecular orientation and electron transfer dynamics at the PTCDA/Au(111) interface using NEXAFS and RPES. PTCDA molecules are found to be lying-down on the substrate with high degree of orientational order. Despite the lying-down geometry of molecules on gold, the charge transfer time scale for both monolayer and multilayer PTCDA is significantly longer than 6 fs as revealed by the core-hole clock spectroscopy. The observed slow charge transfer dynamics is a direct consequence of the weak electronic coupling between PTCDA and Au(111), resulting in a van der Waals type interface.

ACKNOWLEDGMENTS

[1] A. W. Hains, Z. Liang, M. A. Woodhouse, and B. A. Gregg, Chem. Rev. **110**, 6689 (2010).

[2] J. Xue, B. P. Rand, S. Uchida, and S. R. Forrest, Adv. Mater. **17**, 66 (2005).

[3] C. D. Lindstrom and X. Y. Zhu, Chem. Rev. **106**, 4281 (2006).

[4] J. Schnadt, P. A. Brühwiler, L. Patthey, J. N. O'Shea, S. Sodergren, M. Odelius, R. Ahuja, O. Karis, M. Bässler, P. Persson, H. Siegbahn, S. Lunell, and N. Mårtensson, Nature (London) **418**, 620 (2002).

[5] M. Grätzel, MRS Bull. **30**, 23 (2005).

[6] L. Wang, W. Chen, and A. T. S. Wee, Surf. Sci. Rep. **63**, 465 (2008).

[7] L. Wang, L. Liu, W. Chen, Y. Feng, and A. T. S. Wee, J. Am. Chem. Soc. **128**, 8003 (2006).

[8] S. R. Forrest, J. Phys.: Condens. Matter **15**, S2599 (2003).

[9] F. S. Tautz, Prog. Surf. Sci. **82**, 479 (2007).

[10] S. R. Forrest, Chem. Rev. **97**, 1793 (1997).

[11] L. Cao, W. H. Zhang, T. X. Chen, Y. Y. Han, F. Q. Xu, J. F. Zhu, W. S. Yan, Y. Xu, and F. Wang, Acta Phys. Sin. **59**, 1681 (2010).

[12] M. Rohlfing, R. Temirov, and F. S. Tautz, Phys. Rev. B **76**, 115421 (2007).

[13] W. Chen, H. Huang, S. Chen, X. Y. Gao, and A. T. S. Wee, J. Phys. Chem. C **112**, 5036 (2008).

[14] E. L. Moal, M. Müller, O. Bauer, and M. Sokolowski, Phys. Rev. B **82**, 045301 (2010).

[15] S. A. Burke, W. Ji, J. M. Mativetsky, J. M. Topple, S. Fostner, H. J. Gao, H. Guo, and P. Grütter, Phys. Rev. Lett. **100**, 186104 (2008).

[16] W. Chen, H. Huang, S. Chen, L. Chen, H. L. Zhang, X. Y. Gao, and A. T. Wee, Appl. Phys. Lett. **91**, 114102 (2007).

[17] S. M. Barlow and R. Raval, Surf. Sci. Rep. **50**, 201 (2003).

[18] S. Duhm, A. Gerlach, I. Salzmann, B. Bröker, R. L. Johnson, F. Schreiber, and N. Koch, Org. Electron. **9**, 111 (2008).

[19] A. Schmidt, T. J. Schuerlein, G. E. Collins, and N. R. Armstrong, J. Phys. Chem. **99**, 11770 (1995).

[20] H. Vázquez, F. Flores, R. Oszwaldowski, J. Ortega, R. Pérez, and A. Kahn, Appl. Surf. Sci. **234**, 107 (2004).

[21] H. Vázquez, R. Oszwaldowski, P. Pou, J. Ortega, R. Pérez, F. Flores, and A. Kahn, Europhys. Lett. **65**, 802 (2004).

[22] S. Yu, S. Ahmadi, H. Zuleta, H. Tian, K. Schulte, A. Pietzsch, F. Hennies, J. Weissenrieder, X. Yang, and M. Göthelid, J. Chem. Phys. **133**, 224704 (2010).

[23] J. B. Taylor, L. C. Mayor, J. C. Swarbrick, J. N. O'Shea, C. Isvoranu, and J. Schnadt, J. Chem. Phys. **127**, 134707 (2007).

[24] M. P. de Jong, W. Osikowicz, S. L. Sorensen, S. Sergeyev, Y. H. Geerts, and W. R. Salaneck, J. Phys. Chem. C **112**, 15784 (2008).

[25] J. B. Taylor, L. C. Mayor, J. C. Swarbrick, J. N. O'Shea, and J. Schnadt, J. Phys. Chem. C **111**, 16646 (2007).

[26] L. Wang, W. Chen, C. Huang, Z.-K. Chen, and A. T. S. Wee, J. Phys. Chem. B **110**, 674 (2005).

[27] M. P. de Jong, R. Friedlein, S. Sorensen, G. Öhrwall, W. Osikowicz, C. Tengsted, S. Jönsson, M. Fahlman, and W. Salaneck, Phys. Rev. B **72**, 035448 (2005).

[28] W. Chen, L. Wang, D. C. Qi, S. Chen, X. Y. Gao, and A. T. S. Wee, Appl. Phys. Lett. **88**, 184102 (2006).

[29] S. Neppl, U. Bauer, D. Menzel, P. Feulner, A. Shaporenko, M. Zharnikov, P. Kao, and D. L. Allara, Chem. Phys. Lett. **447**, 227 (2007).

[30] W. Wurth and D. Menzel, Chem. Phys. **251**, 141 (2000).

[31] M. Weston, A. J. Britton, and J. N. O'Shea, J. Chem. Phys. **134**, 054705 (2011).

[32] L. C. Mayor, B. J. Taylor, G. Magnano, A. Rienzo, C. J. Satterley, J. N. O'Shea, and J. Schnadt, J. Chem. Phys. **129**, 114701 (2008).

[33] J. Schnadt, J. N. O'Shea, L. Patthey, L. Kjeldgaard, J. Åhlund, K. Nilson, J. Schiessling, J. Krempaský, M. Shi, O. Karis, C. Glover, H. Siegbahn, N. Mårtensson, and P. A. Brühwiler, J. Chem. Phys. **119**, 12462 (2003).

[34] M. Coville and T. D. Thomas, Phys. Rev. A **43**, 6053 (1991).

[35] P. A. Brühwiler, O. Karis, and N. Mårtensson, Rev. Mod. Phys. **74**, 703 (2002).

[36] T. Graber, F. Forster, A. Schöll, and F. Reinert, Surf. Sci. **605**, 878 (2011).

[37] D. A. Outka and J. Stöhr, J. Chem. Phys. **88**, 3539 (1988).

[38] J. Stöhr, *NEXAFS spectroscopy* (Springer-Verlag, Berlin, 1992).

[39] X. Yu, O. Wilhelmi, H. O. Moser, S. V. Vidyaraj, X. Gao, A. T. S. Wee, T. Nyunt, H. Qian, and H. Zheng, J. Electron. Spectrosc. Relat. Phenom. **144–147**, 1031 (2005).

[40] J. Taborski, P. Väterlein, H. Dietz, U. Zimmermann, and E. Umbach, J. Electron. Spectrosc. Relat. Phenom. **75**, 129 (1995).

[41] Y. Zou, L. Kilian, A. Schöll, T. Schmidt, R. Fink, and E. Umbach, Surf. Sci. **600**, 1240 (2006).

[42] W. Chen, D. C. Qi, Y. L. Huang, H. Huang, Y. Z. Wang, S. Chen, X. Y. Gao, and A. T. S. Wee, J. Phys. Chem. C **113**, 12832 (2009).

[43] I. Chizhov, A. Kahn, and G. Scoles, J. Cryst. Growth **208**, 449 (2000).

[44] S. Mannsfeld, M. Toerker, T. Schmitz-Hübsch, F. Sellam, T. Fritz, and K. Leo, Org. Electron. **2**, 121 (2001).

[45] T. Schmitz-Hübsch, T. Fritz, F. Sellam, R. Staub, and K. Leo, Phys. Rev. B **55**, 7972 (1997).

[46] J. Stöhr and D. A. Outka, Phys. Rev. B **36**, 7891 (1987).

[47] M. Sing, J. Meyer, M. Hoinkis, S. Glawion, P. Blaha, G. Gavrila, C. S. Jacobsen, and R. Claessen, Phys. Rev. B **76**, 245119 (2007).

[48] A. C. Liu, J. Stöhr, C. M. Friend, and R. J. Madix, Surf. Sci. **235**, 107 (1990).

[49] C. Mainka, P. S. Bagus, A. Schertel, T. Strunskus, M. Grunze, and C. Wöll, Surf. Sci. **341**, L1055 (1995).

[50] B. N. Holland, N. Peltekis, T. Farrelly, R. G. Wilks, G. Gavrila, D. R. T. Zahn, C. McGuinness, and I. T. McGovern, Phys. Status. Sol. B **246**, 1546 (2009).

[51] J. Schnadt, J. N. O'Shea, L. Patthey, J. Krempaský, N. Mårtensson, and P. A. Brühwiler, Phys. Rev. B **67**, 235420 (2003).

[52] Y. Hirose, A. Kahn, V. Aristov, P. Soukiassian, V. Bulovic, and S. R. Forrest, Phys. Rev. B **54**, 13748 (1996).

[53] Y. Azuma, T. Hasebe, T. Miyamae, K. K. Okudaira, Y. Harada, K. Seki, E. Morikawa, V. Saile, and N. Ueno, J. Synchrotron Radiat. **5**, 1044 (1998).

[54] J. Schnadt, J. Schiessling, and P. A. Brühwiler, Chem. Phys. **312**, 39 (2005).

[55] D. Qi, W. Chen, X. Gao, L. Wang, S. Chen, K. P. Loh, and A. T. S. Wee, J. Am. Chem. Soc. **129**, 8084 (2007).

[56] See supplementary material http://dx.doi.org/10.1063/1.3656834 for more detailed information about RPES spectra and selected RPES spectra at spectator resonant regime as a function of KE.

[57] P. Vilmercati, D. Cvetko, A. Cossaro, and A. Morgante, Surf. Sci. **603**, 1542 (2009).

[58] A. Bendounan, F. Forster, A. Schöll, D. Batchelor, J. Ziroff, E. Umbach, and F. Reinert, Surf. Sci. **601**, 4013 (2007).

[59] A. J. Britton, A. Rienzo, J. N. O'Shea, and K. Schulte, J. Chem. Phys. **133**, 094705 (2010).